Journal of Physics: Conference Series

PAPER • **OPEN ACCESS**

2-Dimensional Regional Mapping of Ionospheric Total Electron Content Using Kriging Interpolation over the Philippines: Initial Results

To cite this article: Vincent Louie L. Maglambayan *et al* 2021 *J. Phys.: Conf. Ser.* **1936** 012012

2-Dimensional Regional Mapping of Ionospheric Total Electron Content Using Kriging Interpolation over the Philippines: Initial Results

Vincent Louie L. Maglambayan[1]*, Merlin M. Mendoza[2], Ernest P. Macalalad[1]

1 Department of Physics, Mapua University, Intramuros, Manila 1002 Philippines
2 Department of Space Science and Engineering, National Central University, Taoyuan City 32001 Taiwan (R.O.C.)
*Email: vlouiem1998@gmail.com

Abstract. Total electron content (TEC) is an important parameter in studying the characteristics of the ionosphere of the Earth. By measuring the phase and group delays of the signals produced by Global Navigation Satellite System (GNSS) satellites, the slant TEC along the ray path can be measured. Assuming that the ionosphere is a thin shell, the point of intersection between the shell and the ray path is the ionospheric pierce point (IPP). The slant TEC at this point can be converted to the vertical TEC (VTEC). To produce continuous 2-dimensional TEC maps, a mapping method must be used based on the data that has been measured. While there are numerous methods to map TEC that are in used today, this study investigates the performance of Kriging interpolation over the Philippine region using the data from the Philippine Active Geodetic Network (PAGENet). To test the performance, the maps produced were compared to the Global Ionosphere Maps (GIMs) which are provided by the International GPS Service (IGS). The initial results show that the PAGENet maps have lower TEC values compared to GIMS with a mean difference of ~6 TECU with 12 UT having the highest difference.

1. Introduction

The ionosphere is the layer of the Earth's upper atmosphere containing free electrons and ionized plasma. which is caused by solar radiation. Ionization varies temporally and spatially. The density of electrons in this layer can affect the propagation of radio waves. Satellite positioning and navigation can lead to errors and less precise readings due to this [1, 2].

Total electron content (TEC) is used in determining the number of electrons found at any given area in the ionosphere. TEC is defined as the line integral of electron density along a ray path between satellite and receiver. Global Navigation Satellite System (GNSS) satellites send signals to receiver stations found all over the globe and measure the delay of these signals. This delay can be used to calculate the TEC at the ray path. Global Ionospheric Maps (GIMs) have been provided by the International GPS Service (IGS) which uses actual TEC data from GNSS satellite observations. This could be used to study the behaviour of TEC in the ionosphere. GIMs have a spatial resolution of 2.5 ° and 5.0 ° in latitude and longitude respectively and a 2-hour temporal resolution [3].

Numerous interpolation methods have been used to map ionospheric TEC. One of those methods is Kriging. This method was originally used for mining data, but it was developed to deal with the spatial

and temporal correlation of data [4]. In a study by Wielgosz et al. [5], they used Kriging and Multiquadratic methods to map regional ionospheric TEC, with data from Ohio CORS stations, and compare them with GIMs. Both methods produced maps with higher temporal and spatial resolution compared to GIMs and found that it is suitable for sparse samplings. Orús et al. used Kriging to improve the Technical University of Catalonia (UPC) GIMs which was computed using GPS data [3]. They found that their improved GIM has lower RMS compared to IGS GIM. They also improved the IGS GIM the same way and found an increase in performance by about 2.5% [6].
The aim of this study is to produce ionospheric TEC maps using Kriging from GNSS-derived TEC from the Philippine Active Geodetic Network (PAGENet) and IGS. These maps are then compared with GIMs and investigate their differences. Previous studies have shown that PAGENet can be used to study latitudinal response of total electron content through various space weather influences such as TEC depletion and scintillation [7, 8]. Thus, this work is an initial step towards analysing such phenomena in a two-dimensional perspective.

2. Methodology

A total of 11 continuously operating GNSS receiver stations operated by PAGENet and 1 IGS GNSS receiver stations in the country were used to observe the TEC around the region. Figure 1 shows the location of these receiver stations. In this initial work, ionospheric TEC maps using Kriging interpolation within the region shown in Figure 1 are produced from a 24-hour GNSS observation on March 14, 2015 at 3-hour intervals. This day has a Kp-index of 2+ which means it is a geomagnetically quiet day. The shell height was set to 350 km with an elevation mask of 25°.

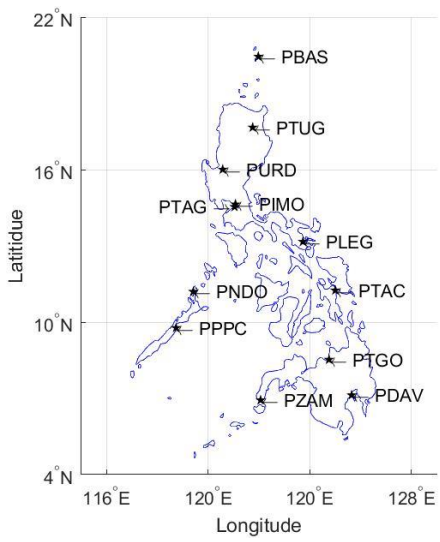

Figure 1. Location of receiver stations. The range of TEC observations both latitudinally and longitudinally were considered and thus, these stations were specifically chosen.

The maps produced have 0.5° by 0.5° resolution and are compared with IGS GIM maps. Here, Kriging-derived maps are subtracted from IGS Maps to calculate the absolute differential TEC. Regional average and standard deviation are also calculated to assess the initial performance of the produced maps.

2.1. Calculation of TEC along the ray path

Phase and group delays depend on the total electron content along the ray path and the radio frequency.

$$-d_p = d_g = \frac{40.3(TEC)}{f^2} \tag{1}$$

where $-d_p$ and d_g are the phase and group delays, respectively. GNSS satellites transmit dual-frequency signals of f_1, 1575.42 MHz, and f_2, 1227.60 MHz. GNSS receivers observe the pseudoranges of both

frequencies. The slant TEC (STEC) along the ray path can be calculated by finding the differences in these pseudoranges [9].

$$STEC = \frac{1}{40.3} \frac{f_1^2 f_2^2}{f_1^2 - f_2^2} (\rho_2 - \rho_1) \tag{2}$$

where ρ_1 and ρ_2 are the pseudoranges of the frequencies f_1 and f_2, respectively.

2.2. Estimation of Differential Code Biases

Inherent instrumental biases are bound to cause errors in the calculation of TEC. These errors are known as differential code biases (DCBs). The IGS has provided satellite and IGS receiver biases to correct this problem. However, the study makes use of PAGENet stations and thus, there is a need to estimate the receiver biases of these stations as they are unknown.

A MATLAB code that estimates the unknown receiver DCBs has been developed by Jin et al. (2012) [10]. They compared the DCB values of IGS stations that the code has produced with the DCB values provided by the IGS. The estimated DCB by the code and the DCB by the IGS has shown good agreement having a mean difference of ~0.7 ns and an RMS of ~0.4 ns.

2.3. Calculation of Vertical TEC

Ionospheric maps use vertical TEC (VTEC) instead of slant TEC. Assuming that the ionosphere is a thin shell, STEC can be converted to VTEC by using a mapping function. The intersection between the ray path and ionospheric shell is called the ionospheric pierce point (IPP). We want to find the VTEC at this point.

$$VTEC = STEC \cos \chi' \tag{3}$$

$$\sin \chi' = \frac{R_E}{R_E + h} \sin \chi \tag{4}$$

where χ' and χ are the zenith angles at the IPP and the receiver, respectively. The zenith angle is the angle between the ray path and the vertical axis of the given point. R_E is the radius of the Earth and h is the altitude of the ionospheric shell.

2.4. Elevation Masking

Satellite signals should reach the receiver at a straight path. Obstructions such as buildings can cause the signals to be reflected before it reaches the receiver. This can cause a lot of unwanted noise in the data. Satellites at lower elevation angles are more likely to get interfered by obstructions and thus, these signals are ignored.

2.5. Kriging Interpolation

There are several types of Kriging. This study makes use of ordinary Kriging which is the most common method [4, 11]. A fundamental assumption in geostatistics is the stationarity of spatially distributed data. This means that the expectation of a spatial function $Z(x)$ is constant and does not depend on the position x.

$$\begin{aligned} &\mathrm{E}\left[Z(x)\right] = m \\ &\mathrm{E}[Z(x+h) - Z(x)] = 0 \end{aligned} \tag{5}$$

Another assumption is that the variance between two points only depends on the distance between measurements.

$$\mathrm{var}[Z(x+h) - Z(x)] = \mathrm{E}\left\{[Z(x+h) - Z(x)]^2\right\} = 2\gamma(h) \tag{6}$$

The function $\gamma(h)$ is the semivariogram. The semivariogram describes the spatial correlation of the function $Z(x)$. The parameter h is the distance between two points. Given a known set of n amount of Z data, we can express an unknown data $\hat{Z}$ at a given point x_0 as seen in equation (7) below.

(7)

λ_i are coefficients that are yet to be determined. We want equation (7) to be unbiased and thus we assume that the sum of the coefficients to be 1 as a constraint.

$$\sum_{i=1}^{n} \lambda_i = 1 \tag{8}$$

From equation (6), we find the variance of the difference between the estimated data $\hat{Z}$ and the actual data Z.

$$\mathrm{var}\left[\hat{Z}(x_0) - Z(x_0)\right] = 2\sum_{i=1}^{n} \lambda_i \gamma(x_i, x_0) - \sum_{i=1}^{n}\sum_{j=1}^{n} \lambda_i \lambda_j \gamma(x_i, x_j) - \gamma(x_0, x_0) \tag{9}$$

The variance between the estimated and the actual value must be minimized. The values of λ_i can be determined from equation (9) using the method of Lagrange using the constraint defined in equation (8).

$$L(\lambda, \mu) = 2\sum_{i=1}^{n} \lambda_i \gamma(x_i, x_0) - \sum_{i=1}^{n}\sum_{j=1}^{n} \lambda_i \lambda_j \gamma(x_i, x_j) - \gamma(x_0, x_0) - 2\mu\left(\sum_{i=1}^{n} \lambda_i - 1\right) \tag{10}$$

The Lagrange multiplier is set to μ. Getting the partial derivatives of $L(\lambda, \mu)$ with respect to λ_i, results in the following equation:

$$\sum_{i=1}^{n} \lambda_i \gamma(x_i, x_j) + \mu = \gamma(x_j, x_0) \tag{11}$$

In matrix form,

$$\begin{bmatrix} \gamma(x_1, x_1) & \cdots & \gamma(x_1, x_n) & 1 \\ \vdots & \ddots & \vdots & \vdots \\ \gamma(x_n, x_1) & \cdots & \gamma(x_n, x_n) & 1 \\ 1 & \cdots & 1 & 0 \end{bmatrix} \begin{bmatrix} \lambda_1 \\ \vdots \\ \lambda_n \\ \mu \end{bmatrix} = \begin{bmatrix} \gamma(x_1, x_0) \\ \vdots \\ \gamma(x_n, x_0) \\ 1 \end{bmatrix} \tag{12}$$

By multiplying the inverse of the first matrix on both sides, equation (12) can be solved and will result in the values for the weighting coefficients λ_l [4,6,11].

2.5.1. Semivariogram. The semivariogram is an important element in Kriging interpolation as it is needed in determining the weighting coefficients. The semivariogram can be determined by taking the variances from our pairs of data measurements that are in a certain distance apart [4].

$$\hat{\gamma}(h_j) = \frac{1}{2m(h_j)} \sum_{i=1}^{m(h_j)} \left[Z(x_i) - Z(x_j)\right]^2 \tag{13}$$

The function $m(h_j)$ represents the number of pairs of measurement $Z(x_i)$ separated by distance h that are within the interval $[h_j, h_{j+1}]$ [12]. Equation (13) is the experimental variogram. For the variogram to be used for interpolation, a theoretical variogram is to be developed which is a model of the experimental variogram [4, 6, 11]. Common variogram models used in Kriging are spherical, exponential, and Gaussian functions.

3. Results and Discussion

Figure 2 below shows the initial maps produced by Kriging interpolation using PAGENet GNSS data and ionospheric GIM maps. The spatial resolution used to map GNSS data is 0.5 ° by 0.5 ° in latitude and longitude. Here, both maps show the typical diurnal variation of TEC where is high from 0 UT to 12 UT with peak at around 9 UT and it is low for the rest of the day. However, Kriging maps show some detailed local features of ionospheric TEC that would is not visible in the smoother GIM maps. This can probably be attributed to clustered distribution of IPPs [5]. Also, Kriging-derived map used 12 stations compare to only 3 stations (PIMO, PTAG and PPPC) using by IGS to produce GIM. Thus, the maps produced by Kriging may be used investigate more detailed features of the ionosphere which may not be possible using GIMs [5]. It should be noted that the day used was on a quiet day. More geomagnetically active days may yield different results. As previously mentioned in section 2, the type of Kriging used in this study is ordinary Kriging. However, other Kriging types might show more reliable results compared to ordinary Kriging. Ordinary Kriging works best when the sample is more scattered and smaller sample size [12].

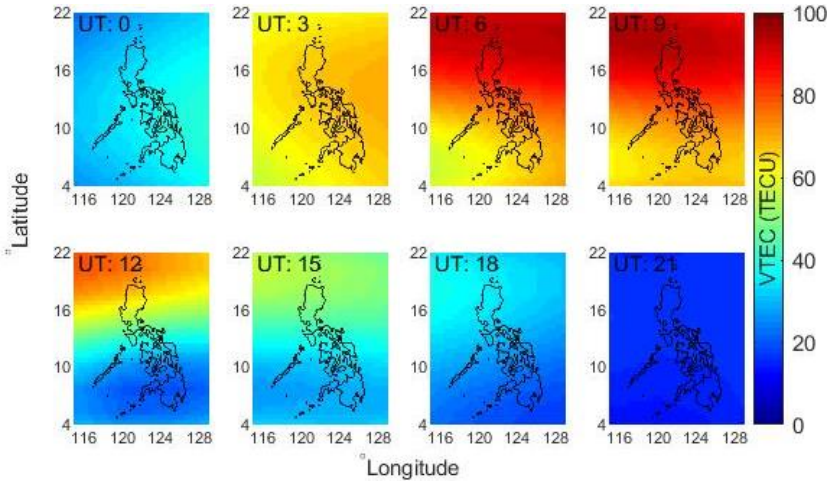

(a)

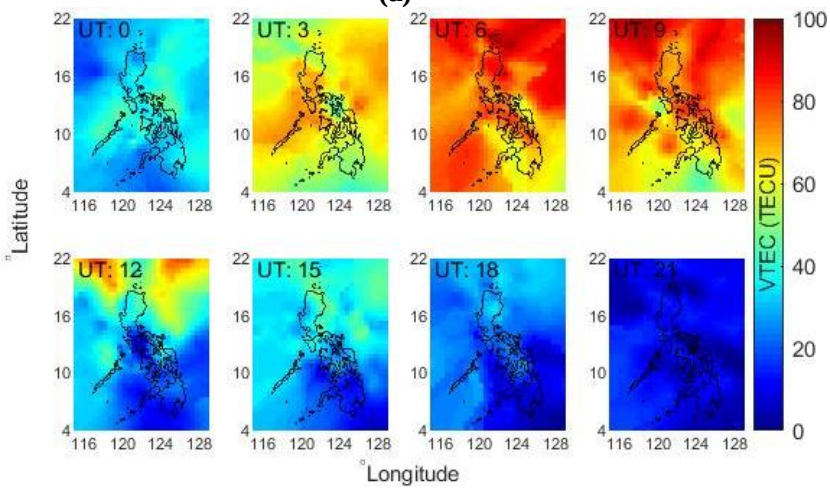

(b)

Figure 2. Ionospheric Maps produced by (a) Kriging interpolation and (b) GIM on March 14, 2015 from 0 UT to 21 UT at 3-hur intervals.

To further compare how much Kriging and GIM differs, the differences between the two were determined and mapped. Figure 3 below shows the differences between Kriging and GIM as well as the distribution of IPPs. GIM generally tends to have higher values compared to Kriging, especially around 12 UT. This could mainly be a cause of the global nature of GIMs, as well as their lower

sampling rate [9]. Most of the areas surrounded with IPPs at a reasonable distance seem to yield differences close to zero as opposed to areas that are close to an IPP. However, further evaluation is needed to confirm this.

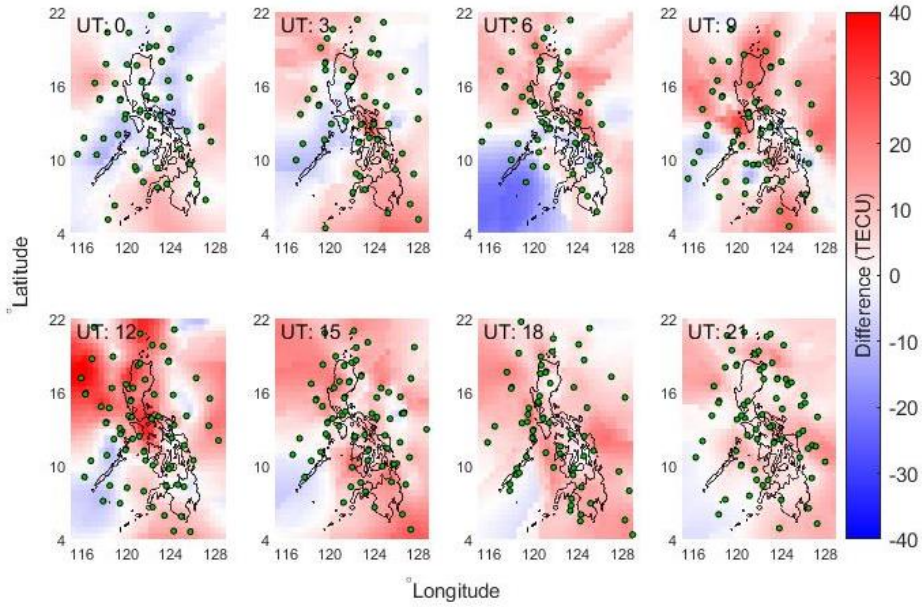

Figure 3. Differences between GIM and Kriging maps with IPPs. Positive difference means that GIM has a higher value compared to the value produced by Kriging and vice-versa for negative differences.

Figure 4 shows the diurnal variation of regional average and standard deviation (error bar) of TEC values using Kriging and GIM on March 14, 2015. The average and standard deviation of the difference between the two maps in this region is also shown. Here, GIM is generally higher than Kriging-derived TEC map with an average difference of about 6.0 TECU. The differences are at its highest post-sunset hours of 12 and 15 UT. This may be attributed to the scintillation events in these period as reported by Juadines et. al. [7]. This suggests that these kinds of features may not be observable using GIM. Further investigation and evaluation should be made during different geomagnetic and ionospheric conditions.

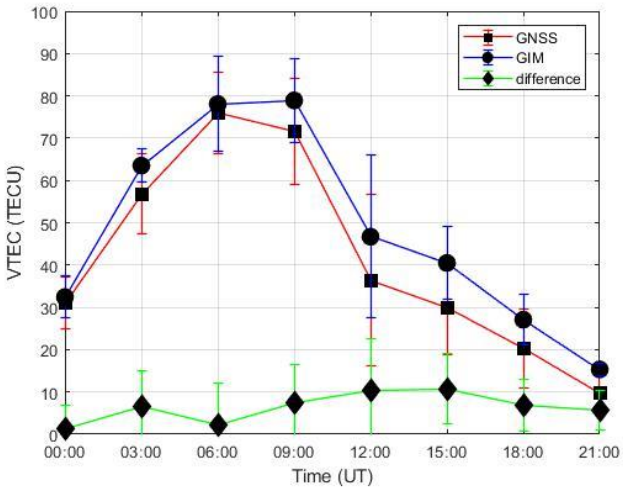

Figure 4. Average TEC of GNSS map (Kriging) and GIM throughout the day. Their differences are also included.

4. Summary and Recommendations

As stated in the discussion above, the mean difference between Kriging maps and GIMs are at ~6.0 TECU with GIMs generally having larger values compared to Kriging. This is possibly due to GIM's global distribution of GNSS receiver stations. As a result, the sampling rate produced by their regional maps are much lower compared to our PAGENet GNSS stations which produced more dense observation points. Another difference is the spatial resolution applied to the GNSS map. While GIMs use a spatial resolution of 2.5 ° latitude and 5.00 ° longitude, the Kriging maps used in this study have a spatial resolution of 0.5 ° by 0.5 ° in both latitude and longitude.

One disadvantage of using Kriging, however, is when observation points are clustered together in a specific subregion. Subregions with little to no data points may result in less reliable TEC values. Thus, the distribution of GNSS receiver stations must properly cover the region to be observed. Other Kriging methods could also yield more reliable results as previously mentioned. It is also important to note that the results shown are initial results and can still be improved including the use of other analysis methods.

Testing with other Kriging methods is also recommended. Further study is needed regarding the performance of this method during geomagnetically active days. In addition, there are more stations that are available from PAGENet. Utilizing these additional stations may improve the quality of mapping that will be produced. Finally, other ways to evaluate the produced maps should be used other than direct comparison with GIM and other available maps. This may include using these in correcting single-frequency GNSS positioning [13, 14, 15].

5. References

[1] Nayir H, Arikan F., Arikan O. and Erol CB 2017 *J. Geophys. Res. Sp. Phys.*, **112** 1–11
[2] R. S. Calfas RS, Garner TW, Harris RB, Gallagher H, Gaussiran TL II and Tolman BW 2008 *Adv. Sp. Res*., **42** 720–726
[3] Orús R, Hernández-Pajares M, Juan JM, Sanz J, García-Fernández M 2002 J Atmos Terr Phys **64** 2055–2062
[4] Cressie NAC 1993 *Statistics for Spatial Data, Revised Edition* (New Jersey: John Wiley & Sons, Inc.)
[5] Wielgosz P, Grejner-Brzezinska D and Kashani I 2003 *J. GPS* **2** 48–55
[6] Orús R, Hernándes-Pajares M, Juan J M and Sanz J 2005 *J. Atm. Solar-Terrestrial Phy.* **67** 1598–1609
[7] Mendoza MM, Macalalad EP, and Juadines KE 2019 *Proc. 2019 6th Int. Conf. on Space Science and Communication* 182-185, 8905982
[8] Juadines KE, Macalalad EP, and Mendoza MM 2019 *Proc. 2019 6th Int. Conf. on Space Science and Communication* 112-115, 8905976
[9] Arikan F, Nayir H, Sezen U and Arikan O 2008 *Radio Science* **43** RS4004
[10] Jin R, Jin S and Feng G 2012 *GPS Solut.* **16** 541–548
[11] Huang L, Zhang H, Xu P, Geng J and Wang C 2017 *Sensors* **17** 468
[12] Blanch J and Walter T 2002 *Proc. ION NTM (San Diego)* 719–724
[13] Macalalad EP, Tsai LC and Wu J 2016 *GPS Sol* **20** 173-185
[14] Macalalad EP, Tsai LC, WU J and Liu CH 2013 *GPS Sol* **17** 337-346
[15] Allain DJ and Mitchell CN 2009 *GPS Sol* **13** 141-151

Acknowledgement

The authors would like to thank the National Mapping and Resource Information Authority (NAMRIA) of the Philippines for providing Philippine Active Geodetic Network (PAGENet) data from their GNSS receivers. The authors would also like to thank the International GNSS Service for providing the GIMs and GNSS data.